Reprinted with permission from: Bakaic E, Smeets NMB, Badv M, Dodd M, ,Barrigar O, Siebers E, Lawlor M, Sheardown H, Hoare T.Injectable and Degradable Poly(Oligoethylene glycol methacrylate) Hydrogels with Tunable Charge Densities as Adhesive Peptide-Free Cell Scaffolds ACS Biomater. Sci. Eng. 2018, 4, 3713−3725 DOI: 10.1021/acsbiomaterials.7b00397

Injectable and Degradable Poly(Oligoethylene glycol methacrylate) Hydrogels with Tunable Charge Densities as Adhesive Peptide-Free Cell Scaffolds

Emilia Bakaic,[†] Niels M.B. Smeets,[†] Maryam Badv,[‡] Megan Dodd,[†] Owen Barrigar,[†] Emily Siebers,[§] Michael Lawlor,[§] Heather Sheardown,[†] and Todd Hoare*,[†]

[†]Department of Chemical Engineering and [‡]School of Biomedical Engineering, McMaster University, 1280 Main Street West, Hamilton, Ontario L8S 4L8, Canada

[§]Department of Pathology and Laboratory Medicine and Neuroscience Research Center, Medical College of Wisconsin, 8701 Watertown Plank Road, Milwaukee, Wisconsin 53226, United States

ABSTRACT: Injectable, dual-responsive, and degradable poly(oligo ethylene glycol methacrylate) (POEGMA) hydrogels are demonstrated to offer potential for cell delivery. Charged groups were incorporated into hydrazide and aldehydefunctionalized thermoresponsive POEGMA gel precursor polymers via the copolymerization of N,N′-dimethylaminoethyl methacrylate (DMAEMA) or acrylic acid (AA) to create dual-temperature/pH-responsive in situ gelling hydrogels that can be injected via narrow gauge needles. The incorporation of charge significantly broadens the swelling, degradation, and rheological profiles achievable with injectable POEGMA hydrogels without significantly increasing nonspecific protein adsorption or chronic inflammatory responses following in vivo subcutaneous injection. However, significantly different cell responses are observed upon charge incorporation, with charged gels significantly improving 3T3 mouse fibroblast cell adhesion in 2D and successfully delivering viable and proliferating ARPE-19 human retinal epithelial cells via an “all-synthetic” matrix that does not require the incorporation of cell-adhesive peptides.

KEYWORDS: hydrogels, pH-responsive materials, thermoresponsive materials, poly(oligoethylene glycol methacrylate), in situ gelling hydrogels, protein adsorption, cell encapsulation, charged hydrogels, retinal regeneration

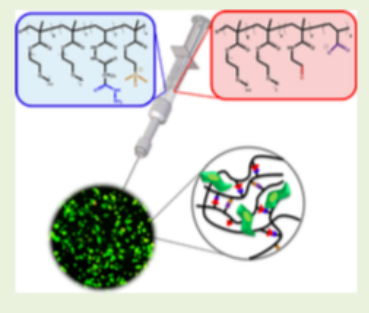

INTRODUCTION

In situ gelling injectable hydrogels have attracted widespread research attention given the practical limitations in using conventional bulk hydrogels in vivo.[1−3] Solutions of lowviscosity gel precursor polymers can be prepared ex vivo containing various drugs, therapeutics, growth factors or cells, and injected in vivo to rapidly form 3-dimensional waterswollen networks useful for filling tissue void defects, delivering drug reservoirs, or transplanting cells.[4,5] Various physical (e.g., temperature,[6,7] ionic,[8] light,[9,10] pressure[11]) and chemical (e.g., in situ click chemistries,[2,12] enzyme mediated[13]) cross-linking approaches have been explored for the design of such materials. The most potentially translatable approaches allow facile chemical modification to tune the physicochemical gel properties, facilitate gelation and degradation in vivo over well-defined time scales, and are either thermodynamically or kinetically bio-orthogonal to avoid or minimize nonspecific protein or tissue interactions and thus subsequent inflammation.

Although several natural[14−16] and synthetic[17−19] polymers have been investigated in this context, stimuli-responsive polymers have demonstrated particular potential as biomedical materials based on their ability to specifically respond to varying physiological stimuli.[6,20,21] Temperature-responsive hydrogels, typically formed by cross-linking polymers exhibiting a characteristic lower critical solution temperature (LCST), enable reversible swelling/shrinking phase transitions at tunable temperatures relative to physiological temperature. For example, the widely known thermoresponsive polymer poly(N-isopropylacrylamide) (PNIPAM) produces hydrogels with a volume phase transition temperature (VPTT) of 32 °C, switching from a swollen hydrophilic matrix at $T < VPTT$ to a less hydrophilic and more collapsed structure at $T > VPTT$.[22] More recently, increasing interest in biomedical applications in particular has focused on poly(oligo ethylene glycol methacrylate) (POEGMA) due to the specific advantages of POEGMA relative to PNIPAM: (1) the VPTT can be tuned precisely from 22 to 90 °C by varying the length of ethylene oxide (EO) repeat units on the side chain;[23] and (2) the degradation products are all generally recognized as safe (GRAS) materials,[24] better facilitating potential clinical translation. The reversible thermoresponsive swelling

properties of such materials have been widely applied in pulsatile or triggered drug delivery applications,[25] whereas the reversible hydrophilicto-(less hydrophilic) transition has been applied to design materials exhibiting reversible cell affinity or switchable cell sheet delamination.[26] In particular, the reversible control over the cell–gel interface provided by thermal switching offers potential benefits in the context of tissue engineering, in which reducing cell reliance on the synthetic matrix as a function of time (as cells make their own matrix) is generally desirable to promote functional tissue regeneration.[26,27] Our group has recently reported extensively on injectable, hydrazone-crosslinked POEGMA hydrogels prepared by coextrusion of hydrazide and aldehyde-functionalized hydrogels that facilitate the minimally invasive delivery of such gels in vivo,[17,21,28] removing a key translational barrier to the use of such materials in the clinic.

pH-responsive hydrogels have also attracted considerable interest given their capacity to reversibly respond to changes in environmental pH, which naturally undergoes substantial variations both as part of normal function (e.g., within the gastrointestinal tract or vagina) or as a response to a diseased state (e.g., in tumors or wounds). pH-responsive hydrogels have been applied to site-specific drug delivery in the stomach[29,30] or the colon,[31] microenvironment-specific delivery responsive to disease,[30] and to promote tissue regeneration through the controlled release of growth factors during cell maturation.[32,33] Most work on the use of such gels in biomedical applications has focused on cross-linking pHsensitive natural (chitosan,[1,34] alginate[35]) and/or synthetic (poly(acrylic acid) (PAA),[36,37] polyethylenimine (PEI) and poly(N,N′-dimethylaminoethyl methacrylate) (PDMAEMA))[38,39] polymers, all of which have different pK_a values, backbone hydrophobicities, and effective ionization ranges to enable tuning of the pH-driven response.[40] Amphoteric gels that contain both cationic and anionic charges have attracted particular attention both due to their demonstrated capacity to suppress nonspecific protein adsorption (thought to be related to their protein-mimetic charge distributions)[41,42] as well as their ability to form ionic cross-links under near-neutral pH conditions in which both the cationic and anionic functional groups are charged,[43] providing an additional cross-linking mechanism to enhance the mechanics of the resulting hydrogels.

Combining the advantageous properties of more than one of these “smart” responses into a single multiresponsive hydrogel can enable additional control over gel properties. For example, Khatoon et al. developed temperature and pH responsive PNIPAM-chitosan hydrogel wound dressings for the release of gentamycin sulfate (GS) that trigger release of the antibiotic as both the temperature and pH of the wound environment was increased; alternatively, we have designed dual-responsive microgels that utilize the thermal phase transition to instantaneously gel at an injection site followed by the pHinduced phase transition to deaggregate and thus release the microgels at a controlled rate.[44] However, to our knowledge, there is no example of a dual thermoresponsive/pH responsive covalently in situ gelling hydrogel that can exploit the benefits of these dual

responses while also being capable of minimally invasive delivery in vivo.

Herein, we report the design of charged, thermoresponsive injectable and degradable POEGMA hydrogels prepared from precursor polymers exhibiting both thermal phase transitions as well as well-defined charge distributions (positive, negative, or amphoteric) that enable both pH-induced phase transitions and pH-tunable secondary (ionic) cross-linking. The dual-responsiveness coupled with the switchable secondary cross-linking is demonstrated to result in hydrogels with substantially broadened swelling, degradation and mechanical profiles amenable to use in biomedical applications; at the same time, no significant increase in nonspecific protein adsorption or chronic tissue responses following subcutaneous injection is observed as a result of charge incorporation, a result attributable to the brush copolymer structure of the POEGMA backbone polymer. We then apply these desirable physicochemical properties to demonstrate the potential of charged POEGMA injectable hydrogels for delivering retinal pigment epithelial (RPE) cells, a potential therapeutic strategy to arrest or reverse vision loss in patients with age-related macular degeneration (AMD) or retinitis pigmentosa (RP) by replacing and stimulating retinal epithelial growth once the native epithelium has been damaged or lost. Given the adhesiondependent properties of RPE cells (which adhere to the basal membrane in vivo for support[45]), polymeric delivery vehicles that can support RPE adhesion while still enabling injection through narrow gauge needles into the back of the eye are essential to translate such therapies to the clinic. The combination of the thermoresponsive POEGMA backbone (facilitating cell interactions without compromising low nonspecific protein adsorption) and charged functional groups (enabling electrostatic interactions between the matrix and the cells) within an injectable platform is demonstrated to support high cell viability and, in some cases, proliferation without cell clumping over extended time periods, as desirable in such a vehicle.

EXPERIMENTAL SECTION

Materials. Oligo(ethylene glycol) methyl ether methacrylate with an average number-average molecular weight of 475 g/mol^{-1} ($OEGMA_{475}$, Sigma-Aldrich, 95%) and di(ethylene glycol) methyl ether methacrylate ($M(EO)_2MA$), Sigma-Aldrich, 95%) were purified using an aluminum oxide packed column (Sigma-Aldrich, type CG-20) to remove the methyl ether hydroquinone (MEHQ) and butylated hydroxytoluene (BHT) inhibitors. N-(2,2-dimethoxyethyl) methacrylamide (DMAEAm, Sigma-Aldrich, 98%) was synthesized according to a previously reported procedure.[17] Acrylic acid (AA, Sigma-Aldrich, 99%), N,N-dimethylaminoethyl methacrylate (DMAEMA, SigmaAldrich 98%), adipic acid dihydrazyde (ADH, Alfa Aesar, 98%), N′ethyl-N-(3-(dimethylamino)propyl)-carbodiimide (EDC, Carbosynth, Compton CA, commercial grade), thioglycolic acid (TGA, SigmaAldrich, 98%), bovine serum albumin (BSA, Sigma-Aldrich, > 96%), fluorescein isothiocyanate (FITC, Sigma-Aldrich, 90%) and 2,2azobisisobutryic acid dimethyl ester (AIBMe, Wako Chemicals, 98.5%) were used as

received. For all experiments, Milli-Q grade distilled deionized water (DIW 18.2 MΩ cm resistivity) was used. Dimethyl sulfoxide (DMSO, reagent grade) was purchased from Caledon Laboratory Chemicals (Georgetown, ON). Hydrochloric acid (1 M) was received from LabChem Inc. (Pittsburgh, PA). Human retinal pigment epithelial cells (ARPE-19) (ThermoFisher Scientific) were expanded in Dulbeccos Modified Growth Medium F12 (DMEMF12, ThermoFisher Scientific) supplemented with 10% fetal bovine serum and 1% Penicillin Streptomycin (ThermoFisher Scientific), and cultured at 37 °C with 5% CO_2 on tissue culture polystyrene (TCPS, Greiner).

Synthesis of Neutral and Charged Hydrazide-Functionalized POEGMA Precursors (POH and POHC). Hydrazide functionalized POEGMA precursor polymers ($PO_{10}H_{30}$) were synthesized as described previously,[28] while cationic hydrazide-functionalized POEGMA precursor polymers ($PO_{10}H_{30}D_{20}$) were synthesized using a modification of that recipe. Briefly, AIBMe (37 mg), $M(EO)_2MA$ (3.9 g), $OEGMA_{475}$ (0.10 g), cationic functional monomer DMEAMA (0 µL for $PO_{10}H_{30}$, 1290 µL for $PO_{10}H_{30}D_{20}$), AA (523 µL for $PO_{10}H_{30}$, and 714 µL for $PO_{10}H_{30}D_{20}$), and TGA (7.5 µL) were dissolved in 1,4dioxane (20 mL). Additional AA was added in the cationic precursor recipe to maintain an equivalence between the number of AA residues per chain (and thus degree of hydrazide functionalization) between neutral and cationic precursors, enabling matching of the reactive functional group contents and thus cross-linking potential in each precursor. After purging for 30 min, the flask was sealed and submerged in a preheated oil bath at 75 °C for 4 h under magnetic stirring. The solvent was removed, and the resulting dry polymer was dissolved in 100 mL DIW. Adipic acid dihydrazide (4.33 g for $PO_{10}H_{30}$, 6.85g for $PO_{10}H_{30}D_{20}$), was added, the pH was lowered to pH 4.75 using 0.1 M HCl, and then EDC (1.93 g for $PO_{10}H_{30}$, 2.44g for $PO_{10}H_{30}D_{20}$) was added, with the pH maintained at pH 4.75 by the dropwise addition of 0.1 M HCl over the subsequent 4 h. The solution was left to stir overnight, dialyzed (MWCO = 3500 g mol^{-1}) against DIW for a minimum of 6 cycles, and lyophilized. The polymers were stored as 20 w/w% solutions in PBS at 4 °C. The degree of functionalization was determined from conductometric base-into-acid titration (ManTech Associates), using a 0.1 wt % polymer solution in 1 mM NaCl as the sample and 0.1 M NaOH as the titrant. Hydrazide polymers are labeled using the convention $PO_xH_yC_z$, where x equals the mole fraction of $OEGMA_{475}$ among the PEG-based monomers added (the remainder of which is $M(EO)_2MA$), y equals the mol % of total monomer residues functionalized with hydrazide reactive groups, and z denotes the mol % of charged monomer incorporated into the polymer.

Synthesis of Neutral and Charged Aldehyde-Functionalized POEGMA Precursors (POA and POAD). Aldehyde functionalized POEGMA precursor ($PO_{10}A_{30}$) was synthesized as described previously,[28] whereas anionic aldehyde functionalized POEGMA precursor ($PO_{10}A_{30}C_{20}$) was synthesized using a modification of that recipe. Briefly, AIBMe (50 mg), $M(EO)_2MA$ (3.9 g), $OEGMA_{475}$ (0.10 g), acetal functional monomer DMAEAm (1.30 g for $PO_{10}A_{30}$, 1.80 g for $PO_{10}A_{30}D_{20}$), anionic functional monomer AA (0 g for $PO_{10}A_{30}$, 0.52 g for $PO_{10}A_{30}C_{20}$), and TGA (7.5 µL) were dissolved in 1,4-dioxane (20 mL). Similar to the hydrazide polymer synthesis, the DMAEAm content was adjusted to ensure an equivalent number of aldehyde

groups and thus cross-linking potential per polymer chain produced. After purging for at least 30 min, the flask was sealed and submerged in a preheated oil bath at 75 °C for 4 h under magnetic stirring. The solvent was removed, and the polymer was subsequently dissolved in 100 mL of 0.5 M HCl. The solution was left to stir for 24 h, dialyzed (MWCO = 3500 g mol^{-1}) against DIW for a minimum of 6 cycles, and lyophilized. The polymers were stored as 20 w/w% solutions in PBS at 4 °C. The degree of functionalization was determined from ^{1}H NMR analysis, comparing the integral values of the -OCH_3 signal (3H, δ = 3.35–3.45 ppm) and the – CHO signal (1H, δ = 9.50–9.58 ppm). Aldehyde polymers are labeled using the convention $PO_xA_yD_z$, where x equals the mole fraction of $OEGMA_{475}$ among the PEG-containing monomers (the remainder of which was $M(EO)_2MA$), y equals the mol % of total monomer residues functionalized with aldehyde reactive groups, and z denotes the mol % of charged monomer incorporated into the polymer.

Synthesis of Fluorescein-Labeled Proteins. Fluorescein-isothiocyanate (FITC)-labeled bovine serum albumin (BSA-FITC) and FITC labeled lysozyme (Lyz-FITC) were prepared by dissolving 50 mg of the protein in a 100 mL carbonate buffer at pH 9.0. FITC (1 mg) was then added, and the solution was incubated at room temperature for at least 12 h under gentle mechanical agitation. The FITC-labeled proteins were subsequently dialyzed against deionized water for 6+ cycles and lyophilized. The isolated conjugated proteins were stored at –4 °C in the dark.

Chemical Characterization of Precursor Polymers. Polymer molecular weight was measured via size exclusion chromatography (SEC) using a Waters 2695 separations module equipped with a Waters 2996 photodiode array detector, a Waters 2414 refractive index detector, a Waters 2475 multi λ fluorescence detector and four Polymer Laboratories PLgel individual pore size columns maintained at 40 °C, with 5 μm bead size and pore sizes of 100, 500, 103, and 105 Å. Tetrahydrofuran (THF) was used as the eluent at a flow rate of 1.0 mL/min, and polystyrene standards were used to calibrate the instrument. Aldehyde contents were measured via ^{1}H NMR using a Bruker AVANCE 600 MHz spectrometer and deuterated chloroform as the solvent. Cloud point temperatures of the polymer precursors and VPTT values of the hydrogels were measured using a Variant Cary Bio 100 UV–vis spectrophotometer. The polymers were dissolved at a concentration of 1 mg/mL in PBS (pH 7.4), and the absorbance of the polymer solution was recorded at 500 nm at every 0.5 °C over a temperature range of 10 to 80 °C (temperature change of 1 °C/min).

Hydrogel Bulk Gel Formation and Gelation Kinetics. Both neutral and charged hydrogels were prepared via coextrusion of hydrazide-functionalized (POH or POHC) and aldehyde-functionalized (POA or POAC) precursors dissolved at 75 mg/mL in 10 mM PBS using a double barrel syringe with a static mixer at the outlet to ensure intensive mechanical mixing (Medmix L series, 2.5 mL volume capacity). The recipes for the bulk hydrogels prepared are shown in Table 2. Hydrogel disks for all benchtop tests (swelling, degradation and VPTT measurements) were prepared by extruding the reactive polymer precursors through the double barrel syringe directly into cylindrical silicone rubber molds (diameter = 7 mm, volume = 300 μL), with gels incubated at room temperature for at least 4 h to ensure complete gelation prior to testing. Hydrogels for cell and protein adsorption studies were extruded directly into the wells of a 96-well polystyrene multiwell plate, while hydrogels for in vivo experiments were injected directly into the

subcutaneous space.

Gelation times were assessed by extruding 200 μL of the reactive precursor solutions at concentrations of 75 mg/mL in PBS into a 2 mL microcentrifuge tube that is rotated manually every 5 s. The gelation time is defined as the time point at which the hydrogel visually no longer flows on the time scale of the rotation (5 s).

Hydration and Swelling. Hydrogel swelling was determined gravimetrically at 37 °C in 10 mM citrate, phosphate and carbonate buffered solutions of pH 3, 7.4, and 10 respectively. Hydrogels were placed into cell culture inserts that were subsequently placed into a 12well cell culture plate and completely submerged with PBS (4 mL/ well). At predetermined time intervals, the cell culture inserts were removed from the well, the PBS was drained, and the hydrogel was gently dried to wick off nonabsorbed PBS. The hydrogel disks were then weighed, after which the hydrogels were resubmerged into a fresh 4 mL of PBS solution and tested repeatedly until equilibrium swelling was reached (generally ~30 h). Error bars represent the standard deviation of the replicate measurements (n = 4). The mass-based swelling ratio (Q_m) was calculated by dividing the mass of the hydrogel at any given time point (m_h) by the dry mass of polymer in the hydrogel (m_p = initial hydrogel mass × (1 − water content)).

Hydrolytic Degradation. Hydrogel degradation was determined gravimetrically in acid-accelerated conditions at 37 °C in the presence of 100 mM HCl (pH 1.0); these acid-catalyzed conditions were used to compare the degradation properties of the hydrogels on a more measurable time frame as well as assess specifically the role of hydrazone hydrolysis (catalyzed in acidic conditions)[46] on the relative degradation times of the gels. Hydrogels were placed into cell culture inserts that were subsequently placed in a 12-well cell culture plate and completely submerged in the HCl solution (4 mL per well). At predetermined time intervals, the cell culture inserts were removed from the well, excess solution was drained, and the hydrogel was gently wicked off to remove any nonabsorbed solution prior to weighing the hydrogel. Hydrogels were then resubmerged in fresh HCl solution (4 mL/well) until the hydrogel was completely degraded (i.e., no separate phase was observed between the hydrogel and the HCl bath solution). Error bars represent the standard deviation of the replicate measurements (n = 4).

Rheology. The rheological properties of the hydrogels were measured using an ARES rheometer (TA Instruments) operating under parallel-plate geometry with a plate diameter of 7 mm and a plate spacing of 1 mm. Rheological properties were measured by first conducting a strain sweep from 0.1–100% strain at 1 Hz to identify the linear viscoelastic range of the hydrogels. A strain was then selected within this range and set as a constant to perform a frequency sweep from 1 to 100 rad/s to measure shear elastic (G′) and loss (G″) moduli. All measurements were conducted at 25 °C, with error bars representing the standard deviation of the replicate measurements (n = 3).

In Vitro Protein Absorption. To assess whether protein uptake was occurring primarily via adsorption or absorption, larger gel samples (for which absorption would be more prevalent) of cylindrical shape and volume 300 μL were formed in a 3.5 mm radius silicone mold and left to gel completely for 4 h. Protein uptake into the hydrogel disks was measured by placing the gels into cell culture inserts and subsequently in a 12-well cell culture plate, completely submerging

the gel in a 5 mg/mL BSA-FITC solution (4 mL per well). After 2 h, the cell culture inserts and gels were removed from the well and a 300 μL sample of the residual BSA-FITC solution was transferred into a 48-well plate and quantified using fluorescence as previously described. Based on the initial weight of polymer present in each gel, a μg/mg BSA uptake of polymer was calculated. Each experiment (hydrogels as well as controls) was done in quadruplicate, with reported errors representing the standard deviation of the replicates.

In Vitro Protein Adsorption. To differentiate between interfacial adsorption and bulk absorption, we conducted thin film hydrogel adsorption assays in 96-well plates. POH/POHC/POA/POAC polymer solutions (75 mg/mL) were first sterilized by passing the solutions through a 0.2 μm filter, after which 30 μL of each precursor solution was extruded into each well of the 96 well plate and left overnight to ensure complete gelation. Following, 180 μL of 10 mM PBS was added to each well, and hydrogels were allowed to swell to equilibrium prior to protein addition for 30 h (a time confirmed to correspond to equilibrium swelling for all hydrogels tested, see Figure 1B). Excess PBS was then removed, and 60 μL of either BSA-FITC or lysozyme-FITC solution at concentrations of 125, 250, 500, or 1000 μg/mL in PBS was added. The hydrogels were incubated for 2 h at 37 °C, after which the hydrogels were rigorously rinsed five times with 10 mM PBS to remove unadsorbed protein and the fluorescence signal was measured using a VICTOR 3 multilabel microplate reader using an excitation wavelength of 495 nm and an emission wavelength of 535 nm; linear calibration curves ($R^2 > 0.99$) were observed in the concentration ranges of 1 to 10 μg/mL and 10 to 100 μg/mL for BSAFITC and lysozyme-FITC respectively. Each experiment (hydrogels as well as controls) was done in quadruplicate, with reported errors representing the standard deviation of the replicates.

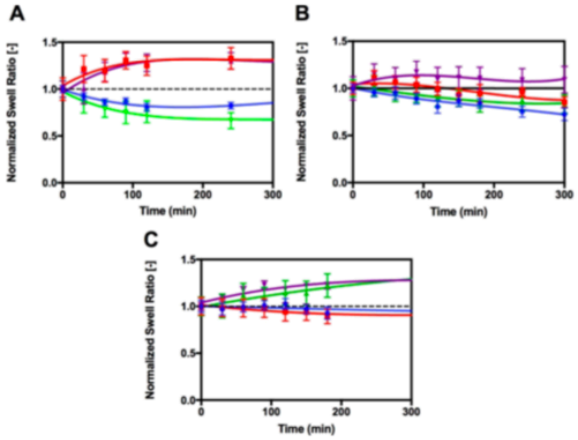

Figure 1. Swelling kinetics of POEGMA hydrogels in 10 mM (A) citrate buffer, pH 3; (B) phosphate buffer, pH 7.4; and (C) carbonate buffer, pH 10 at 37 °C: (blue) PO_{10}, (red) PO_{10}-cat, (purple) PO_{10}-amp, (green) PO_{10}-an. Lines are guides to the eye.

Precursor Polymer Cytotoxicity. Cell cytotoxicity of the charged POEGMA precursor polymers was evaluated using a rezasurin assay with varying exposure concentrations to 3T3 mouse fibroblasts. Briefly, 3T3 mouse fibroblasts were plated at a density of 10 000 cells/ well in a 96 well polystyrene tissue culture plate. The 96 well plates were then incubated for 24 h at 37 °C in DMEM supplemented with FBS (10%) and penicillin/streptomycin (1%). After incubation, cells were exposed to varying concentrations of charged hydrazide and aldehyde precursor polymer ranging from 100 to 1000 μg/mL and the plate was incubated for another 24 h. Cytotoxicity was assessed through the addition of 10 μg/mL resazurin reagent. After 2 min of subsequent

incubation at 37 °C, the fluorescence of each well was measured using a VICTOR 3 multilabel microplate reader using an excitation wavelength of 495 nm and an emission wavelength of 535 nm. Viabilities were determined by subtracting background fluorescence readings (blank well with no cells) from each well and then calculating the ratio of the signal intensity of polymer-exposed cells to untreated cell controls (no polymer exposure) (n = 4).

Cell Morphology on 2D Hydrogels. The cell morphology of mouse 3T3 fibroblasts was assessed on the surface of the charged POEGMA hydrogels. Hydrogels were directly extruded into each well of a 48-well plate (100 μL of each sterilized polymer precursor solution prepared at 150 mg/mL in 10 mM PBS), leaving the gel overnight to ensure complete gelation. Gels were then incubated at 37 °C in 600 μL of sterilized 10 mM PBS and allowed to equilibrate for 24 h prior to cell plating to ensure equilibrium swelling was achieved prior to cell plating. The PBS was then removed, and gels were washed with DMEM culture media prior to cell addition. Cells were plated on top of the hydrogels at a density of 1.0×10^4 cells per well together with 600 μL of DMEM and incubated for 48 h at 37 °C. After the incubation period, a LIVE/DEAD assay was conducted to visualize cells using microscopy and quantify adhesion. Each well was washed three times with sterile 10 mM PBS to remove any nonadherent cells from the gels before staining. Fluorescent live cells were imaged for morphological characterization and counted using a Zeiss Axiovert 200 M fluorescence/live cell imaging microscope, using ImageJ for image analysis. All experiments were conducted in quadruplicate, with multiple images (n = 4) taken per well for analysis; error ranges report represent the standard deviation associated with the total cell counts (across the multiple images taken per replicate) in the replicate measurements.

In Vivo Subcutaneous Injections. All animals received care that complied with protocols approved by the Animal Research Ethics Board at McMaster University and the guidelines of the Canadian Council on Animal Care. The in vivo response of the injectable charged hydrogels was assessed histopathologically following subcutaneous injection of the charged hydrogels using autoclaved double barrel syringes into male BALB/c mice (Charles River, Montreal; 22– 24 g weight). Precursor polymer solutions (75 mg/mL) were filtered using a 0.2 mm syringe filter, loaded into an autoclaved double barrel syringe under aseptic conditions, and injected subcutaneously in the scruff of the neck at a volume of 0.3 mL total gel volume/mouse. Mice were anesthetized using isoflurane prior to injection to ensure reproducible injection sites and substantial gelation prior to mouse movement. Following visual tracking of mouse behavior and health during the experiment, animals were euthanized by carbon dioxide asphyxiation after acute (2 days) and chronic (30 days) time points. Tissue samples from around the injection site were recovered, fixed in formalin, and stained with eosin and hematoxylin. Inflammatory responses to the hydrogels were assessed using two methods: (1) local leukocyte concentrations adjacent to the hydrogel (indicative of material-induced inflammation) were determined through ImageJ analysis (n = 4 for every material tested, 4 images analyzed per mouse); and (2) a histological scoring system was used to semiquantitatively describe the intensity of inflammation, where 0 = normal, 1 = no acute/chronic inflammation other than macrophages prior to fat and other subcutaneous tissue, 2 = inflammation without necrosis, 3 = focal inflammation with some necrosis, 4 = widespread inflammation with significant necrosis, 5 = massive inflammation.

ARPE-19 3D Cell Encapsulation. Human retinal cells (ARPE-19) at passage 8 were rinsed with

PBS, detached from the plate surface with TrypLE Express Enzyme (TypLE, ThermoFisher Scientific), resuspended in complete DMEM-F12 media, and centrifuged to pelletize the cells. Supernatant media was carefully removed, and pelleted cells were resuspended directly in the hydrazide-containing $PO_{10}H_{30}$ and $PO_{10}H_{30}D_{20}$ precursor polymers at a concentration of 2.5×10^6 cells/mL. In advance, 15 μL of the corresponding aldehydecontaining $PO_{10}A_{30}$, and $PO_{10}A_{30}C_{20}$ precursor polymers was aliquoted to individual wells on coverslip bottom, 96-well plates. Aliquots (15 μL) of the hydrazide $PO_{10}H_{30}$ and $PO_{10}H_{30}D_{20}$ precursor suspensions containing ARPE-19 cells were then added to the complementary aldehyde polymer-containing wells and rapidly mixed via pipet aspiration. ARPE-19 cells were identically resuspended in 15 μL of Geltrex LDEV-Free Reduced Growth Factor Basement Membrane Matrix (Geltrex, ThermoFisher Scientific) and aliquoted to wells containing 15 μL of Geltrex to serve as a control with the same overall cell number. Both the test and control gels were allowed to gel for 2 h at 37 °C. Following, 120 μL of DMEM containing 10% FBS and 1% penicillin streptomycin was placed on top of each gel and the gels were incubated for up to 2 weeks to track cell viability, with media replaced every 2–3 days. Cell morphology and viability was measured via confocal microscopy (Nikon Eclipse Ti), with image processing conducted using NIS Elements and ImageJ. A z-stack depth of 200 μm was scanned for each sample. Cells were fluorescently labeled using a live/dead assay by removing the media and adding 50 μL of live–dead solution consisting of 2 μM calcein AM (calcein, Sigma-Aldrich) and 4 μM ethidium homodimer-1 (EthD-1, Sigma-Aldrich) in PBS. Cells were incubated for 30 min prior to imaging. Quantitative live cell numbers were determined using a VICTOR 3 multilabel microplate reader and reading the fluorescence using an excitation wavelength of 495 nm and an emission wavelength of 535 nm. Fluorescence intensities in relative fluorescence units were determined by subtracting background fluorescence readings (blank gel with no cells) from each well (n = 6).

RESULTS

Synthesis. Charged poly(oligoethylene glycol methacrylate) (POEGMA) hydrogel precursors were synthesized via chain transfer agent-mediated free radical copolymerization of oligoethylene glycol methacrylate monomers with varying ethylene glycol side chain lengths (n). Each multiresponsive prepolymer was prepared by copolymerizing one functional monomer to allow covalent cross-linking via hydrazide/aldehyde chemistry and another functional monomer to impart charge into the polymer (AA for anionic precursor polymers or DMAEMA for cationic precursor polymers) (Scheme 1). The 90:10 monomer ratio between diethylene glycol methacrylate ($M(EO)_2MA$, n = 2) and oligoethylene glycol methacrylate ($OEGMA_{475}$ n = 8–9) used to prepare all precursor polymers was selected to produce (unfunctionalized) POEGMA polymers with a target LCST similar to PNIPAM (~32 °C), providing the desired thermosensitivity in the resulting copolymers. Each hydrazide $PO_xH_yC_z$ and $PO_xA_yD_z$ precursor reported in this paper was functionalized with a targeted y = 30 mol % functional hydrazide or aldehyde functional groups (such that the theoretical cross-link density in each hydrogel formed is equivalent regardless of how the different precursor

polymers are mixed) and, where present, z = 20 mol % charged monomer. Conductometric titration confirms ~20 mol % charged monomer content in both $PO_{10}H_{30}C_{20}$ and $PO_{10}A_{30}D_{20}$ as well as ~30 mol % hydrazide functionalization in both $PO_{10}H_{30}$ and $PO_{10}H_{30}C_{20}$ (Table 1); however, the actual aldehyde incorporation into both $PO_{10}A_{30}$ and $PO_{10}A_{30}D_{20}$ was slightly lower than the stoichiometric expectation at ~22–24 mol %, a result we attribute to lower potential incorporation of acetal monomer during copolymerization. However, despite this lower aldehyde functionalization, the similar degree of functionalization of both aldehyde-functionalized precursors means that the potential for cross-link formation is the same between any pair of precursor polymers tested. As such, the hydrogels formed from these precursors polymers are expected to be chemically equivalent aside from the incorporation or exclusion of charged monomers. The number-average molecular weight (M_n) of the polymer precursors is also consistent between the different precursors and is controlled to be less than 20×10^3 g/mol (Table 1), well below the renal clearance limit of $40–50 \times 10^3$ g/mol to facilitate polymer elimination following gel degradation.

Scheme 1. Synthesis of Charged POEGMA Precursor Polymers

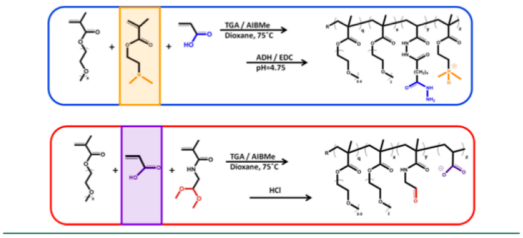

Table 1. Chemical Characterization of Synthesized Charged POEGMA Polymer Precursors

hydrogel	$M(EO)_2MA$ (mol %)	$OEGMA_{475}$ (mol %)	functional reactive group	functional reactive monomer (mol %)	charged group	functional charged monomer (±) (mol %)
$PO_{10}H_{30}$ (POH)	60.2	6.7	$NHNH_2$	33.1[a]	N/A	
$PO_{10}H_{30}C_{20}$ (POH-cat)	39.3	4.4	$NHNH_2$	33.1[a]	DMAEMA	(+)18.4 ± 2.1[a]
$PO_{10}A_{30}$ (POA)	70.6	7.8	CHO	21.6[b]	N/A	
$PO_{10}A_{30}D_{20}$ (POA-an)	53.5	4.1	CHO	23.9[b]	AA	(−) 17.3 ± 3.5[a]

[a]Determined from conductometric titration. [b]Determined by ^{1}H NMR

Physiochemical Properties. Hydrogels were prepared by coextruding binary combinations of hydrazide-functionalized (POH/POHC) and aldehyde-functionalized (POA/POAD) precursor polymers dissolved at 75 mg/mL in 10 mM PBS using a double barrel syringe to form neutral, cationic, amphoteric and anionically charged gels (Table 2). All binary combinations of precursor polymers gelled rapidly, between <5 to 45 s (Table 2). The effect of charge was significantly different depending on the type and combination of charged precursor polymers used. Cationic hydrogels prepared with a cationic hydrazide precursor and a neutral aldehyde precursor exhibited slower gelation times than the neutral networks with the same backbone composition, a result anticipated based on the electrostatic repulsion between the cationic DMAEMA residues of adjacent precursor polymers. On the other hand, amphoteric hydrogels consisting of a mixture of cationic hydrazide precursor polymer and anionic aldehyde precursor polymer gelled significantly faster than the neutral combination, consistent with ionic attractions as well as covalent gelation driving interpolymer interactions in this system. Interestingly, hydrogels prepared with a neutral hydrazide precursor and an anionic aldehyde precursor gelled

significantly faster than the neutral combination, on par with the amphoteric formulation that is aided by electrostatic interactions.

Table 2. Preparation of Charged POEGMA Hydrogels

POEGMA hydrogel			hydrazide precursor		aldehyde precursor	
hydrogel	charge	gelation time (s)	precursor	concentration(mg/mL)	precursor	concentration(mg/mL)
PO_{10}	neutral	30	$PO_{10}H_{10}$	75	$PO_{10}A_{10}$	75
PO_{10}-cat	cationic	45	$PO_{10}H_{10}D_{20}$	75	$PO_{10}A_{10}$	75
PO_{10}-amp	amphoteric	<5	$PO_{10}H_{10}D_{20}$	75	$PO_{10}A_{10}C_{20}$	75
PO_{10}-an	anionic	<5	$PO_{10}H_{10}$	75	$PO_{10}A_{10}C_{20}$	75

The effect of charge on hydrogel swelling was quantified at 37 °C in buffers of 10 mM pH 3 (citrate), pH 7.4 (phosphate) and pH 10 (carbonate) over a time period of 30 h (Figure 1); these pH values were chosen based on the pK_a values of both charged comonomers (AA $pK_a = 4.3$, DMAEMA $pK_a = 8.5$) such that only the cationic comonomer would be charged (pH 3), only the anionic monomer would be charged (pH 10), and both monomers would be charged (physiological pH 7.4). At pH 3 (Figure 1A), the cationic and amphoteric gels swell relative to their prepared state, the former due to ionization and the latter due to effective de-cross-linking of the ionic network as the AA residues are protonated; in contrast, the neutral gel deswells slightly (attributable to the slightly higher ionic strength at pH 3) and the anionic gel collapses as – COOH groups are protonated and hydrogen bonding interactions with residual hydrazide groups are promoted. At pH 10, the anionic gel swells due to –COOH ionization, whereas the amphoteric gel also swells again due to disruption of the ionically crosslinked network (here, following DMAEMA deprotonation, leaving only anionic charged groups); the neutral gel remains near its initial volume while the cationic gel deswells slightly due to enhanced hydrogen bonding following functional group neutralization. Intermediate swelling behaviors were observed at pH 7.4, with the amphoteric gel shrinking the most over time consistent with the development of an ionically cross-linked secondary network in the gel over time. Thus, the swelling profiles confirm the anticipated pH-responsive behavior of POEGMA hydrogels prepared with functionalized precursor polymers and our capacity to tune the charge type/content of the gels by simple mixing of functionalized precursor polymers.

The effect of charge incorporation on temperature response of the hydrogels was then quantified at the same pH values tested for swelling by a stepwise temperature ramp from 20 to 50 °C at 5 °C intervals, allowing 12 h between temperature steps to ensure that equilibrium conditions were reached for each temperature measurement (Figure 2). At pH 7.4, the characteristic collapse profile of the neutral PO_{10} gel with a VPTT of ~32–33 °C (similar to NIPAM) is observed; a similar phase transition is observed in the cationic PO_{10}-cat hydrogel, given that deprotonation of the cationic groups ($pK_a \approx 8.5$) is partially complete at physiological pH and the effective charge density on the gel is lower. However, the fully ionized anionic gel (ionic repulsion and higher bound water content) and the amphoteric gel (ionic cross-linking) both undergo much slower and less extreme phase transitions, consistent with observations on conventional charged hydrogels.[47] At pH 3, the hydrazone bond is labile over ~96 h course of the full temperature ramp, leading to effective gel degradation in the cationic and amphoteric gels (both of which are

more swollen and thus accessible to acid degradation at pH 3, Figure 1A) as the temperature is ramped. This result is consistent with the accelerated 0.1 M HCl degradation results (Figure 3), which indicate rapid swelling and subsequent degradation over time for the cationic and amphoteric gels but rapid collapse followed by extremely slow degradation of the collapsed network for the anionic and neutral gels. Alternately, at pH 10, the ester bond linking the ethylene oxide side chain to the methacrylate backbone in each gel tested is labile over the same time frame (Figure S3); consequently, the volume phase transition is suppressed in each gel tested due to the generation of ionized methacrylate residues on the backbone polymer as degradation occurs.

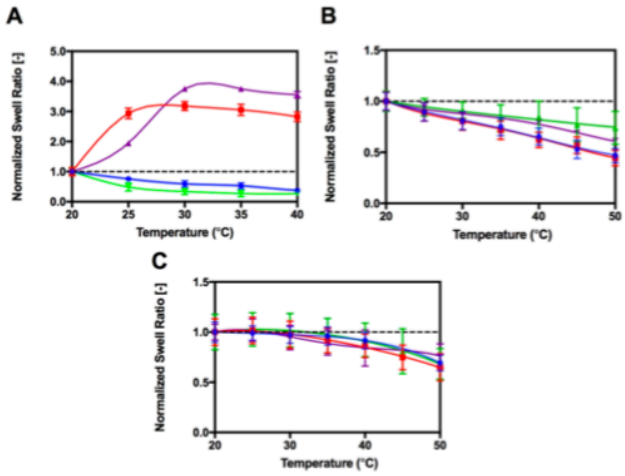

Figure 2. Swelling kinetics of POEGMA hydrogels in pH 3, 7.4, or 10 buffers as a function of temperature: (blue) PO_{10}, (red) PO_{10}-cat, (purple) PO_{10}-amp, (green) PO_{10}-an. Lines are guides to the eye.

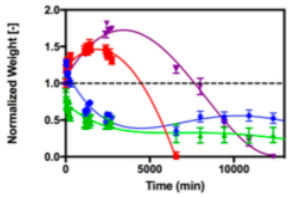

Figure 3. Degradation profiles of POEGMA hydrogels in 0.1 M HCl solution at 37 °C: (blue) PO_{10}, (red) PO_{10}-cat, (purple) PO_{10}-amp, (green) PO_{10}-an. Lines are guides to the eye.

The rheological properties of the charged POEGMA gels are shown in Figure 4. The plateau elastic storage modulus (G′) increases with the incorporation of charge, with both cationic (~1160 ± 160 Pa) and anionic (~1650 ± 360 Pa) gels exhibiting higher elasticity relative to hydrogels prepared without charge (~820 ± 140 Pa). This result is consistent with an increase in bound water within the charged hydrogels, with the higher effective charge density in the anionic gel relative to the cationic gel at pH 7.4 resulting in a slightly higher enhancement in the anionic gel modulus. However, in the dual ionic–covalent cross-linked amphoteric gel, the contribution of the second electrostatic network results in a significant increase in the shear storage modulus (~2820 ± 370 Pa), an ~3.5-fold increase in G′ compared to the neutral gel consistent with the presence of

dual cross-linking.

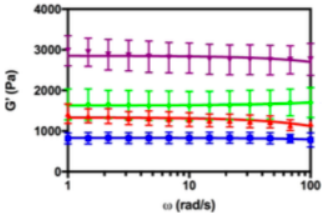

Figure 4. Average elastic storage moduli (G') of the fully swollen mixed precursor POEGMA hydrogels in 10 mM PBS at 37 °C: (blue) PO_{10}, (red) PO_{10}-cat, (purple) PO_{10}-amp, (green) PO_{10}-an. Lines are guides to the eye.

In Vitro Cytocompatibility. To assess the biological potential of these hydrogels, the cytocompatibility of the charged polymer precursors was first assessed using a rezasurin cell viability reagent assay on 3T3 mouse fibroblasts to ensure the precursor polymers themselves did not negatively impact cells (Figure 5). Neither the cationic nor anionic precursor polymers (which also represent the degradation products posthydrolysis) showed any cytotoxicity at concentrations up to 1000 μg/mL, analogous to the noncharged control precursor polymers. This result is important since cationic polymers in particular often exhibit cytotoxicity, particularly at the relatively high polymer concentrations tested in Figure 5; this is not problematic in the cationic POEGMA polymers.

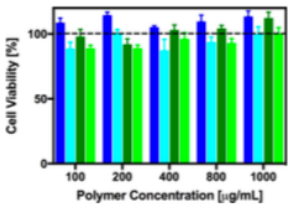

Figure 5. Resazurin cell viability assay of POEGMA precursor polymers after 24 h incubation with 3T3 mouse fibroblasts at 37 °C: $PO_{10}H_{30}$ (blue), $PO_{10}H_{30}C_{2.0}$ (light blue), $PO_{10}A_{30}$ (dark green), $PO_{10}A_{30}D_{20}$ (green).

In Vitro Protein Affinity. To assess the inflammatory potential of charged POEGMA hydrogels, the affinity between the charged hydrogels and proteins was assessed through two separate assays. First, protein absorption within the hydrogel was measured by fully immersing templated bulk cylindrical gels (surface area:volume ratio = 0.8:1) in a BSA solution and, without rinsing, removing the hydrogels and measuring the residual BSA content in solution (Table 3). In this case, protein uptake into the charged gels is uniformly higher than the corresponding neutral gel, with the cationic gel exhibiting higher uptake than the anionic gel (consistent with the net anionic charge of BSA at physiological pH) and the amphoteric gel exhibiting highest uptake (consistent with the effective total charge density in the amphoteric gel being double the other two charged hydrogels, Table 2). Thus, from an absorption perspective, the charged POEGMA hydrogels behave similarly to previously reported charged gels in which the presence of

more charge enhances protein uptake.

Table 3. BSA uptake into charged POEGMA hydrogels from 70 μg/mL BSA stock solution in 10 mM PBS (37°C)

hydrogel	[BSA] in stock solution after 48 h (μg/mL)	μg BSA/mg polymer in gel
PO_{10}	57 ± 9	0.3 ± 0.2
PO_{10}-cat	43 ± 5	0.6 ± 0.1
PO_{10}-amp	24 ± 4	1.3 ± 0.2
PO_{10}-an	29 ± 7	1.0 ± 0.2

Following, a protein adsorption experiment was performed on thin film hydrogels constrained within a 96-well plate (surface area:volume ratio 1.8:1) (Figure 6). Both lysozyme and BSA were tested at various concentrations, with 15 sequential PBS rinses performed to remove any absorbed or weakly bound protein prior to assaying the residual gel fluorescence. As such, this assay was designed to probe the interfacial interactions between the gels and proteins, which are more critical to predicting inflammatory potential.[48] Typically, introducing charge (and particularly cationic charge) significantly increases the amount of protein deposition on a biomaterial surface due to electrostatic interactions with either the net charge or local charged domains of proteins. For BSA (66 kDa, pI ≈ 4.8), the cationic gel adsorbs slightly more protein than the neutral gels, consistent with expectations; however, both the anionic and amphoteric gels adsorb less protein than even the neutral POEGMA gel. For lysozyme, (14 kDa, pI ≈ 11.3), protein adsorption is similar between all hydrogels tested irrespective of charge, despite net charge attraction between lysozyme and the anionic gel. Thus, very low protein adsorption is maintained regardless of incorporation of even 10 mol % charge in the hydrogels. This result is consistent with the brushlike PEG side-chains tethered on the POEGMA backbone assisting in masking the charges located closer to the backbone to maintain very low protein adsorption in all cases. This is also consistent with the very low cytotoxicity of the cationic precursor polymer measured (Figure 5) and represents a potential advantage of these injectable POEGMA materials in that a large fraction of charges can be introduced to affect other gel properties (e.g., swelling, thermoresponsivity, mechanics, etc.) without significantly affecting protein adsorption.

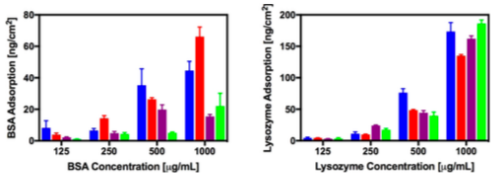

Figure 6. Protein adsorption to charged POEGMA hydrogels in 10 mM PBS at 37 °C: (A) bovine serum albumin; (B) lysozyme: (blue) PO_{10}, (red) PO_{10}-cat, (purple) PO_{10}-amp, (green) PO_{10}-an.

In Vitro Cell Adhesion. To assess the impact of introducing charge on the capacity of cells to adhere to the hydrogels, cell adhesion of 3T3 mouse fibroblasts was assessed following the plating of 10 000 cells/well on top of the same thin film hydrogel samples used for the protein adsorption tests (Figure 7).

Significantly more cells adhered to all of the charged hydrogels (Figure 7B–D) relative to the neutral (uncharged) PO_{10} hydrogel (Figure 7A). This result indicates that charge promotes cell adhesion to otherwise highly cell-repellent POEGMA hydrogels without the need to incorporate additional bioadhesive functional groups. The PO_{10}-cat cationic hydrogel (Figure 7B) shows particularly high cell adhesion consistent with the electrostatic attraction induced between the 3T3 cells and the hydrogel interface; indeed, the total fluorescence (related to number of live cells counted) on PO_{10}-cat is only ~20% lower than that of the tissue culture polystyrene control (Figure 7E), albeit with significantly higher cell clumping observed indicative of weaker cell electrostatic interactions instead of stronger binding interactions that can promote more focal adhesions with the gel interface.[49,50] Thus, charged POEGMA hydrogels can support the adhesion and proliferation of viable cells despite the low nonspecific protein binding observed to these materials (Figure 6).

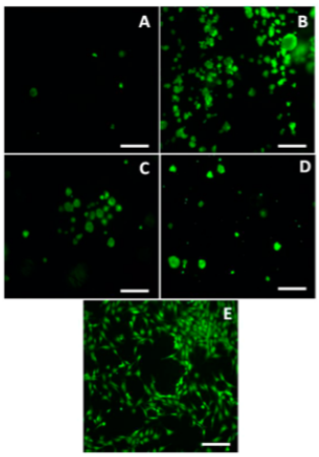

Figure 7. Adhesion of mouse 3T3 fibroblasts to charged POEGMA hydrogels following 48 h of incubation: (A) PO_{10} (neutral), (B) PO_{10}-cat (cationic), (C) PO_{10}-amp (amphoteric), (D) PO_{10}-an (anionic), (E) tissue culture polystyrene control. Scale bar = 100 μm.

Subcutaneous in Vivo Tissue Compatibility. To assess the tissue compatibility of the charged POEGMA hydrogels in vivo, subcutaneous injections of the PO_{10}, PO_{10}-cat, PO_{10}-amp and PO_{10}-an hydrogels were performed using BALB/c mice (Figure 8). Each binary combination rapidly (<1 min) formed a hydrogel when injected, consistent with in vitro observations, and no obvious signs of skin irritation were noted in any of the mice injected. Injection of the PO_{10}, PO_{10}-cat, PO_{10}-amp and PO_{10}-an hydrogels resulted in moderate infiltration of leukocytes to the hydrogel-tissue interface at the acute (2 day) time point, with both the anionic (490 ± 220 cells mm^{-2}) and in particular the amphoteric (450 ± 180 cells mm^{-2}) gels exhibiting comparable inflammatory responses to the neutral PO_{10} gel (~500 cells mm^{-2}). The cationic PO_{10}-cat gel showed a substantially higher presence of polymorphonuclear cells (1200 ± 180 cells mm^{-2}) then all other gels, indicating stronger acute inflammation consistent with the higher BSA adsorption observed (Figure 6A). From histological scoring, all gels exhibited at least localized

inflammatory responses inducing limited cell necrosis (Table 4; see scoring system in Experimental Section).

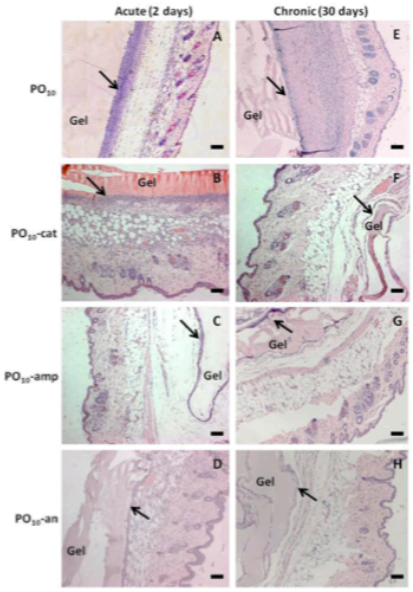

Figure 8. Histological sections of stained subcutaneous tissue samples following injection of (A, E) PO_{10}, (B, F) PO_{10}-cat, (C, G) PO_{10}-amp and (D, H) PO_{10}-an hydrogels following a(A–D) cute and (E–H) chronic time points. Arrows indicate the presence of leukocytes. All hydrogels are still present at chronic time points. Scale bars = 100 μm.

Table 4. Histological Scores for Determination of Severity and Reaction to the Injection of Charged POEGMA Hydrogels into the Subcutaneous Space of BALB/c Mice

	histology score	
hydrogel	acute (2 days)	chronic (30 days)
PO_{10}-cat	4 ± 1	1 ± 0
PO_{10}-amp	4 ± 1	2 ± 1
PO_{10}-an	3 ± 2	1 ± 0

However, no significant difference in score was observed between $PO_{10\text{-cat}}$ and the other gels, indicating that the higher number of leukocytes present does not induce a significant difference in tissue morphology.

At the chronic time point (30 days), all gels persisted in the subcutaneous space but showed evidence of at least some degradation, with cells penetrating between segments of gel in all cases. Only the neutral PO_{10} gel (which appears to be degrading most slowly of the tested gels) showed a considerable decrease in leukocytic concentration, with the polymorphonuclear cell density dropping to ~75 cells mm^{-2} compared to PO_{10}-amp (380 ± 170 cells mm^{-2}) and PO_{10}-an hydrogels (330 ± 100 cells mm^{-2}). This difference is likely related is attributable to the different degradation rates of these gels, leading to different concentrations of leukocytes over time. Of note, the cationic PO_{10}-cat gel shows a similar leukocyte density at the chronic time point relative to the other charged gels (360 ± 90 cells mm^{-2}), suggesting that the larger acute inflammation observed resolves at the chronic time point despite the continuing presence (and degradation) of the cationic

hydrogel. Thus, while the cationic PO_{10}-cat gel induces higher acute inflammation, the chronic inflammatory response remains mild; this result is significant based on the large inflammatory responses often observed with cationic biomaterials.[51] This significant resolution of an inflammatory response is further confirmed through histological scoring, in which scores of 1 (PO_{10}, $PO_{10\text{-cat}}$, and $PO_{10\text{-an}}$, indicating no inflammation aside from a few macrophages due to ongoing gel degradation) or at most 2 ($PO_{10\text{-A}}$, indicative of a macrophage response associated with gel degradation but no cell necrosis) were observed. It should also be emphasized that no clear evidence of fibrosis (or "walling off" of the gels) is observed for any of the injected gels after 30 days, significant for the potential use of these materials for controlled release applications for either cells or therapeutics. Furthermore, there is clear evidence of gel degradation in each chronic histology image presented, with the presence of charge (and in particular cationic charge) appearing to accelerate the breakup of the bulk gel into fragments surrounded by degrading inflammatory cells. This result confirms the degradability of these materials in vivo, with the rate of degradation observed optionally engineered by the density of reactive hydrazide/ aldehyde functional groups and the concentration of the precursor polymers injected.[28]

3D Cell Encapsulation. Given the demonstrated potential of these charged POEGMA gels as injectable biomaterials, we next investigated the potential of leveraging both the thermoresponsivity and the charge of the hydrogels for creating delivery vehicles for human retinal pigment epithelial cells (ARPE-19) that are injectable, degradable, and do not require the inclusion of bioadhesive biomolecules to support cell adhesion or proliferation. ARPE-19 cells were coextruded with the charged and neutral POEGMA gel precursor polymers at a concentration of 2.5×10^6 cells/mL; cell viability and morphology was tracked over 15 days and compared to a commercially available Geltrex hydrogel that consists of natural extracellular matrix components (laminin, collagen IV, entactin, and heparin sulfate) and has been previously used for retinal cell delivery to the back of the eye.[45] All of the POEGMA-based hydrogels tested could support and maintain cell viability over the full 15-day test period, with the cells remaining relatively isolated within the matrix; this is desirable for cell transplantation applications in the retina, as large aggregations of retinal cells during bolus injection lead to high cell death due to nutrient and oxygen suffocation and limited integration into native tissues.[52] In contrast, the Geltrex matrix induced significant clumping of ARPE-19 cells less desirable for cell delivery applications. Plate coverage measurements on live cell fluorescence indicated less proliferation inside the POEGMA gels relative to the Geltrex matrix (Figure 9J); however, the Geltrex matrix fully degraded after 15 days, whereas the POEGMA matrices can still support viable and largely isolated cells.

The benefits of charge incorporation are also observed by comparing the performance of the neutral PO_{10} hydrogel to the charged gels. PO_{10} gels (which show minimal 2D cell adhesion, Figure 7) show a slight decrease in viable cell count between days 3 and 15 as

well as more dead (red) cells in the matrix over time (Figure 9B). In contrast, all the charged hydrogels support cell proliferation within the matrix over the same time period (Figure 9J). Although the number of cells supported is highest in the cationic $PO_{10\text{-}cat}$ gel at all time points (Figure 9C, D), both the anionic $PO_{10\text{-}an}$ and, in particular, the amphoteric $PO_{10\text{-}A}$ gels minimize the number of dead cells and cell clumping observed after 15 days (Figures 9F, H). This trend is also reflected in fluorescence intensity measurements between days 1 and 3 (Figure 10), in which the anionic and amphoteric gels maintain highest cell viability immediately following the delivery process (i.e., at day 1) but support slower cell proliferation; the amphoteric gel in particular maintains highest cell viability at day 1 but supports only minimal cell expansion over following 14 days. This result is consistent with the amphoteric hydrogel having the highest internal cross-linking density among all gels (Figure 4) due to the dual covalent/ionic cross-linking present, resulting in the most mechanical resistance for cell proliferation. The improved capacity of charged hydrogels to support cell adhesion is likely attributable to a combination of direct cell-matrix electrostatic interactions (for hydrogels containing cationic charges only),[43] chargeinduced triggering of the production of more adhesive extracellular matrix protein by the cells themselves,[43,53] and/ or charge-based recruitment of proteins from serum to the hydrogel surface[54] (although, based on the protein adsorption results in Figure 6, this latter factor is likely a minor contributor). However, the exact mechanism of this adhesion enhancement is a subject for future investigation. As such, although all charged POEGMA gels offer promise relative to existing (more expensive and more difficult to purify) options as injectable delivery matrices for retinal epithelial cells, the nature of the charge present can alter the cell response between maintenance and proliferation within the matrix.

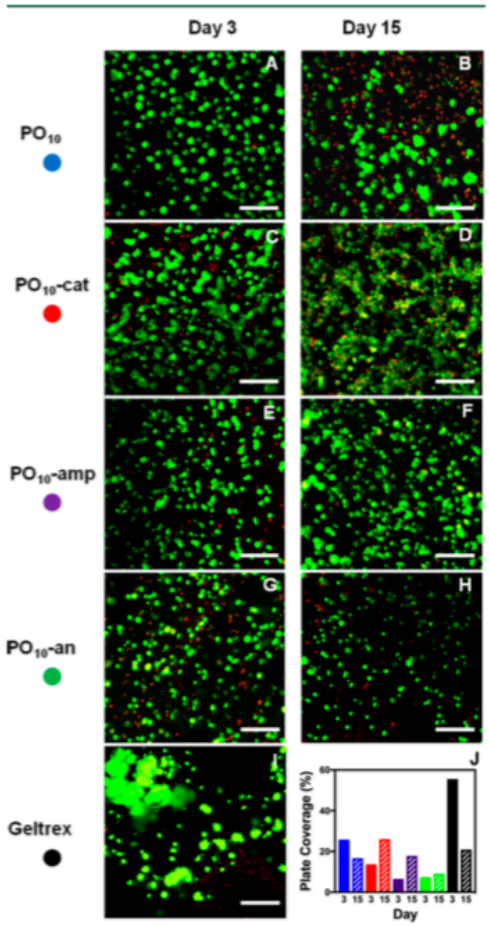

Figure 9. 3D encapsulation of ARPE-19 cells imaged using confocal microscopy (200 μm *z*-stack) after 3 days and 15 days in neutral and charged POEGMA hydrogels: (A, B) PO_{10} (neutral); (C, D) PO_{10}-cat (cationic); (E, F) PO_{10}-amp (amphoteric); (G, H) PO_{10}-an (anionic) (I) Geltrex matrix control. (J) Percentage of fluorescence plate coverage of live cells for each gel and time point. Scale bar = 100 μm.

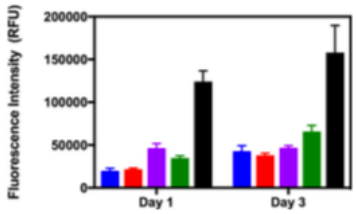

Figure 10. Average fluorescence reading taken using a VICTOR 3 multilabel microplate reader using calcein AM staining of ~19 cells encapsulated within charged POEGMA hydrogels after Day 1 and Day 3 at 37 °C: (blue) PO_{10}, (red) PO_{10}-cat, (purple) PO_{10}-amp, (green) PO_{10}-an, (back) Geltrex.

DISCUSSION

The combination of a thermoresponsive polymer backbone with cationic and/or anionic groups that can be switched on or off as a function of pH leads to an injectable hydrogel formulation with a series of highly tunable properties under different environmental

conditions. All formulations gelled in less than 1 min following coextrusion from a double barrel syringe and formed coherent gels that did not undergo syneresis as gelation proceeded. Uncharged PO_{10} hydrogels showed characteristic thermoresponsive swelling and interfacial responses, while the inclusion of a single type of ionizable functional groups shifts the hydrophilic/hydrophobic balance back to a more hydrophilic state, driving significant positive swelling effects in the case of single charge hydrogels that also facilitate accelerated degradation kinetics. Alternately, amphoteric hydrogels in which both anionic and cationic charges are present facilitate the creation of a secondary ionically crosslinked network, resulting in an effectively dual-cross-linked hydrogel that swells less (Figure 1) and has significantly higher modulus values (Figure 4). Of note, anionically functionalized hydrogels also exhibited somewhat faster gelation (Table 2), stronger mechanics (Figure 4), and slower degradation (similar to the amphoteric hydrogels that have a well-defined secondary networking structure, Figure 3) than the other tested hydrogels, suggesting the presence of an additional networking driving force in these materials. Although hydrogen bonding between lone pair-donating ethers in the ethylene oxide repeat units in the OEGMA side-chains and the lone pair accepting carboxylic acid groups of acrylic acid residues on the anionic POEGMA polymers is the most likely reason for these results,[55] elucidating the exact nature of this interaction requires further study.

The varying physicochemical and mechanical properties achieved via the incorporation of charge in thermoresponsive polymer precursors can subsequently be leveraged to engineer cell and tissue responses to these hydrogels. Inclusion of cationic, amphoteric and/or anionic charge within the POEGMA hydrogels significantly increases cell adhesion of 3T3 fibroblast cells to the matrix relative to neutral hydrogel controls (Figure 7), facilitating cell adhesion without the need for using RGD or other adhesive peptides while still exhibiting low nonspecific protein adsorption relative to other biomaterials or even neutral POEGMA gels (Figure 6). The chronic inflammatory response of each of the hydrogels was mild, even though the gels were continuously degrading to release the functional polymer precursors at the one month chronic time point tested (Figure 8). Furthermore, the successful encapsulation (and later proliferation) of ARPE-19 cells by injection within the charged POEGMA gels (Figure 9) suggests the benefits of this combination of relatively low nonspecific protein adsorption and charge in an injectable cell delivery vehicle, with the charged gels supporting higher cell viabilities and proliferation (albeit to different degrees based on the network structure) compared to neutral POEGMA gels and better suspension of the cells relative to the Geltrex control. Given that cell adhesion via integrin binding can induce specific biological triggers for cells to differentiate[56] and/or otherwise alter internal cytoplasmic signaling,[57] achieving cell adhesion without invoking integrin pathways may be beneficial in certain applications like retinal cell delivery in which avoiding integrin mediated responses (here, cell spreading to form cell clumps observed in Geltrex) is undesirable."

Thus, manipulation of hydrogel charge to effect favorable application-based properties

can be conducted without compromising the compatibility of the materials in vivo. Of note, given that these POEGMA hydrogels can be fabricated by simple mixing, the charge density of the hydrogels can be easily adjusted by mixing neutral and charged precursor polymers of the same functionality (i.e., hydrazide or aldehyde) in the appropriate barrel of the double barrel syringe, a modular design enabling rapid tuning of gel properties ideal for screening gel responses in specific applications. In particular,

the pH-responsive charge densities and swelling properties presented are highly consistent with those of existing pHresponsive hydrogels used in site-specific (e.g., stomach or colon) or disease-specific (e.g., infection site targeting) drug delivery applications, many of which are not injectable (or at least are much less easy to inject). As such, the injectable, degradable, and charge-controlled hydrogels described herein may offer significant benefits in a broader biomedical context.

CONCLUSIONS

Dual-temperature and pH-responsive POEGMA hydrogels offer both physicochemical benefits in terms of highly tunable swelling, degradation, and rheological properties as well as biological benefits in terms of maintaining low nonspecific protein adhesion and promoting both cell adhesion and proliferation. In particular, manipulating the hydrogel charge can significantly improve both the 2D cell adhesive potential of 3T3 mouse fibroblasts and the 3D stabilization and proliferative potential of ARPE-19 human retinal epithelial cells without the need for cell adhesive ligands. Furthermore, the brush structure of POEGMA suppresses both nonspecific protein adsorption and chronic inflammatory responses to the charged hydrogels relative to typical charged hydrogels (particularly for the cationic gels). On this basis, we suggest that these hydrogels offer significant potential as injectable and degradable matrices for in vivo cell delivery.

Supporting Information The Supporting Information is available free of charge on the ACS Publications website at DOI: 10.1021/acsbiomaterials.7b00397.

NMR spectra of all polymers produced (PDF)

Corresponding Author

*E-mail: hoaretr@mcmaster.ca. ORCID Todd Hoare: 0000-0002-5698-8463 Notes

The authors declare no competing financial interest.

ACKNOWLEDGEMENTS

The Natural Sciences and Engineering Research Council of Canada (NSERC) is acknowledged for funding this work (Strategic Project Grant STPGP 447372 and Discovery Grant RGPIN 356609).

REFERENCES

(1) Tan, H.; Chu, C. R.; Payne, K. A.; Marra, K. G. Injectable in Situ Forming Biodegradable Chitosan-Hyaluronic Acid Based Hydrogels for Cartilage Tissue Engineering. Biomaterials 2009, 30, 2499–2506.

(2) Hudson, S. P.; Langer, R.; Fink, G. R.; Kohane, D. S. Injectable in Situ Cross-Linking Hydrogels for Local Antifungal Therapy. Biomaterials 2010, 31, 1444–1452.

(3) Nguyen, M. K.; Lee, D. S. Injectable Biodegradable Hydrogels. Macromol. Biosci. 2010, 10, 563–579.

(4) Wang, H.; Liu, Z.; Li, D.; Guo, X.; Kasper, F. K.; Duan, C.; Zhou, J.; Mikos, A. G.; Wang, C. Injectable Biodegradable Hydrogels for Embryonic Stem Cell Transplantation: Improved Cardiac Remodelling and Function of Myocardial Infarction. J. Cell. Mol. Med. 2012, 16, 1310–1320.

5) Ban, K.; Park, H.; Kim, S.; Andukuri, A.; Hwang, J.; Cho, K.; Cha, H.; Kim, S. S.; Kim, W.-S.; Jun, H.-W.; Yoon, Y.-S. Cell Therapy with Embryonic Stem Encapsulated in Injectable Nanomatrix Gel Enhances Cell Engraftment. ACS Nano 2014, 8, 10815–10825.

(6) Payyappilly, S.; Dhara, S.; Chattopadhyay, S. Thermoresponsive Biodegradable PEG-PCL-PEG Based Injectable Hydrogel for Pulsatile Insulin Delivery. J. Biomed. Mater. Res., Part A 2014, 102, 1500–1509.

(7) Gong, C.; Qi, T.; Wei, X.; Qu, Y.; Wu, Q.; Luo, F.; Qian, Z. Thermosensitive Polymeric Hydrogels as Drug Delivery Systems. Curr. Med. Chem. 2013, 20, 79–94.

(8) Van Tomme, S. R.; Van Steenbergen, M. J.; De Smedt, S. C.; Van Nostrum, C. F.; Hennink, W. E. Self-Gelling Hydrogels Based on Oppositely Charged Dextran Microspheres. Biomaterials 2005, 26, 2129–2135.

(9) Hou, Y.; Schoener, C. A.; Regan, K. R.; Munoz-Pinto, D.; Hahn, M. S.; Grunlan, M. A. Photo-Crosslinked PDMSstar-PEG Hydrogels: Synthesis, Characterization, and Potential Application for Tissue Engineering Scaffolds. Biomacromolecules 2010, 11, 648–656.

(10) Jiang, Y.; Chen, J.; Deng, C.; Suuronen, E. J.; Zhong, Z. Click Hydrogels, Microgels and Nanogels: Emerging Platforms for Drug Delivery and Tissue Engineering. Biomaterials 2014, 35, 4969–4985.

(11) Annabi, N.; Mithieux, S. M.; Weiss, A. S.; Dehghani, F. CrossLinked Open-Pore Elastic Hydrogels Based on Tropoelastin, Elastin and High Pressure CO2. Biomaterials 2010, 31, 1655–1665.

(12) Patenaude, M.; Hoare, T. Injectable, Mixed Natural-Synthetic Polymer Hydrogels with Modular Properties. Biomacromolecules 2012, 13, 369–378.

(13) Moreira Teixeira, L. S.; Leijten, J. C. H.; Wennink, J. W. H.; Chatterjea, A. G.; Feijen, J.; van Blitterswijk, C. A.; Dijkstra, P. J.; Karperien, M. The Effect of Platelet Lysate Supplementation of a Dextran-Based Hydrogel on Cartilage Formation. Biomaterials 2012, 33, 3651–3661.

(14) Matsuno, T. Design of Injectable Bone Tissue Engineering Scaffold Consists of SS-Tricalcium Phosphate Beads and Alginate. Tissue Engineering 2010, 297–307.

(15) Frey, N.; Linke, A.; Süselbeck, T.; Müller-Ehmsen, J.; Vermeersch, P.; Schoors, D.; Rosenberg, M.; Bea, F.; Tuvia, S.; Leor, J. Intracoronary Delivery of Injectable Bioabsorbable Scaffold (IK-5001) to Treat Left Ventricular Remodeling After ST-Elevation Myocardial Infarction: A First-in-Man Study. Circ.: Cardiovasc. Interventions 2014, 7, 806–812.

(16) Hori, Y.; Winans, A. M.; Huang, C. C.; Horrigan, E. M.; Irvine, D. J. Injectable Dendritic Cell-Carrying Alginate Gels for Immunization and Immunotherapy. Biomaterials 2008, 29, 3671–3682.

(17) Smeets, N. M. B.; Bakaic, E.; Patenaude, M.; Hoare, T. Injectable and Tunable Poly(ethylene Glycol) Analogue Hydrogels Based on Poly(oligoethylene Glycol Methacrylate). Chem. Commun. 2014, 50, 3306–3309.

(18) Tai, H.; Howard, D.; Takae, S.; Wang, W.; Vermonden, T.; Hennink, W. E.; Stayton, P. S.; Hoffman, A. S.; Endruweit, A.; Alexander, C.; et al. Photo-Cross-Linked Hydrogels from Thermoresponsive PEGMEMA-PPGMA-EGDMA Copolymers Containing Multiple Methacrylate Groups: Mechanical Property, Swelling, Protein Release, and Cytotoxicity. Biomacromolecules 2009, 10, 2895–2903.

(19) García, A. J. PEG-Maleimide Hydrogels for Protein and Cell Delivery in Regenerative Medicine. Ann. Biomed. Eng. 2014, 42, 312– 322.

(20) Sa-´Lima, H.; Tuzlakoglu, K.; Mano, J. F.; Reis, R. L. Thermoresponsive poly(N-Isopropylacrylamide)-G-Methylcellulose Hydrogel as a Three-Dimensional Extracellular Matrix for CartilageEngineered Applications. J. Biomed. Mater. Res., Part A 2011, 98, 596– 603.

(21) Bakaic, E.; Smeets, N. M. B.; Dorrington, H.; Hoare, T. Off-theShelf" thermoresponsive Hydrogel Design: Tuning Hydrogel Properties by Mixing Precursor Polymers with Different Lower-Critical Solution Temperatures. RSC Adv. 2015, 5, 33364–33376.

(22) Patenaude, M.; Hoare, T. Injectable, Degradable Thermoresponsive Poly(N -Isopropylacrylamide) Hydrogels. ACS Macro Lett. 2012, 1, 409–413.

(23) Lutz, J.-F. Thermo-Switchable Materials Prepared Using the OEGMA-Platform. Adv. Mater. 2011, 23, 2237–2243.

(24) Working, P. K.; Newman, M. S.; Johnson, J.; Cornacoff, J. B. Safety of Poly(ethylene Glycol) and Poly(ethylene Glycol) Derivatives. Poly(ethylene glycol) 1997, 680, 45–57.

(25) Hu, Z.; Cai, T.; Chi, C. Thermoresponsive Oligo(ethylene Glycol)-MethacrylateBased

Polymers and Microgels. Soft Matter 2010, 6, 2115.

(26) Haraguchi, Y.; Shimizu, T.; Yamato, M.; Okano, T. Regenerative Therapies Using Cell Sheet-Based Tissue Engineering for Cardiac Disease. Cardiol. Res. Pract. 2011, 2011, 845170.

(27) Cooperstein, M. A.; Canavan, H. E. Biological Cell Detachment from poly(N-Isopropyl Acrylamide) and Its Applications. Langmuir 2010, 26, 7695–7707.

(28) Smeets, N. M. B.; Bakaic, E.; Patenaude, M.; Hoare, T. Injectable Poly(oligoethylene Glycol Methacrylate)-Based Hydrogels with Tunable Phase Transition Behaviours: Physicochemical and Biological Responses. Acta Biomater. 2014, 10, 4143–4155.

(29) Guo, B.; Finne-Wistrand, A.; Albertsson, A. C. Facile Synthesis of Degradable and Electrically Conductive Polysaccharide Hydrogels. Biomacromolecules 2011, 12, 2601–2609.

(30) Khutoryanskiy, V. V. Advances in Mucoadhesion and Mucoadhesive Polymers. Macromol. Biosci. 2011, 11, 748–764.

(31) Kakoulides, E. P.; Smart, J. D.; Tsibouklis, J. Azocrosslinked Poly(acrylic Acid) for Colonic Delivery and Adhesion Specificity: In Vitro Degradation and Preliminary Ex Vivo Bioadhesion Studies. J. Controlled Release 1998, 54, 95–109.

(32) Matsusaki, M.; Akashi, M. Novel Functional Biodegradable Polymer IV: pH-Sensitive Controlled Release of Fibroblast Growth Factor-2 from a Poly(gamma-Glutamic Acid)-Sulfonate Matrix for Tissue Engineering. Biomacromolecules 2005, 6, 3351–3356.

(33) Wu, D. Q.; Sun, Y. X.; Xu, X. D.; Cheng, S. X.; Zhang, X. Z.; Zhuo, R. X. Biodegradable and pH-Sensitive Hydrogels for Cell Encapsulation and Controlled Drug Release. Biomacromolecules 2008, 9, 1155–1162.

(34)Hoemann,C.D.;Sun,J.;Leǵare,´a;McKee,M.D.;Buschmann, M. D. Tissue Engineering of Cartilage Using an Injectable and Adhesive Chitosan-Based Cell-Delivery Vehicle. Osteoarthritis Cartilage 2005, 13, 318–329.

(35) D'Arrigo, G.; Di Meo, C.; Pescosolido, L.; Coviello, T.; Alhaique, F.; Matricardi, P. Calcium Alginate/dextran Methacrylate IPN Beads as Protecting Carriers for Protein Delivery. J. Mater. Sci.: Mater. Med. 2012, 23, 1715–1722.

(36) Povea, M. B.; Monal, W. A.; Cauich-Rodriguez, J. V.; Pat, A. M.; Rivero, N. B.; Covas, C. P. Interpenetrated Chitosan-Poly(Acrylic Acid-Co-Acrylamide) Hydrogels. Synthesis, Characterization and Sustained Protein Release Studies. Mater. Sci. Appl. 2011, 2, 509–520.

(37) Elliott, J. E.; Macdonald, M.; Nie, J.; Bowman, C. N. Structure and Swelling of Poly (Acrylic Acid) Hydrogels: Effect of pH, Ionic Strength, and Dilution on the Crosslinked Polymer Structure. Polymer 2004, 45, 1503–1510.

(38) van de Wetering, P.; Zuidam, N. J.; van Steenbergen, M. J.; van der Houwen, O. A. G. J.; Underberg, W. J. M.; Hennink, W. E. A Mechanistic Study of the Hydrolytic Stability of Poly

(2(Dimethylamino) Ethyl Methacrylate). Macromolecules 1998, 31, 8063–8068.

(39) Zhai, M.; Chen, Y.; Yi, M.; Ha, H. Swelling Behaviour of a New Kind of Polyampholyte Hydrogel Composed of Dimethylaminoethyl Methacrylate and Acrylic Acid. Polym. Int. 2004, 53, 33–36.

(40) Yan, H.; Jin, B. Influence of Environmental Solution pH and Microstructural Parameters on Mechanical Behavior of Amphoteric pH-Sensitive Hydrogels. Eur. Phys. J. E: Soft Matter Biol. Phys. 2012, 35, 36.

(41) Feng, Z.; Shao, Z.; Yao, J.; Chen, X. Protein Adsorption and Separation on Amphoteric Chitosan/ Carboxymethylcellulose Membranes. J. Biomed. Mater. Res., Part A 2008, 86, 694–700.

(42) Damodaran, V. B.; Murthy, N. S. Bio-Inspired Strategies for Designing Antifouling Biomaterials. Biomater. Res. 2016, 20, 18.

(43) Sun, T. L.; Kurokawa, T.; Kuroda, S.; Ihsan, A. B.; Akasaki, T.; Sato, K.; Haque, M. A.; Nakajima, T.; Gong, J. P. Physical Hydrogels Composed of Polyampholytes Demonstrate High Toughness and Viscoelasticity. Nat. Mater. 2013, 12, 932–937.

(44) Hoare, T.; Young, S.; Lawlor, M. W.; Kohane, D. S. Thermoresponsive Nanogels for Prolonged Duration Local Anesthesia. Acta Biomater. 2012, 8, 3596–3605.

(45) Parker, J.; Mitrousis, N.; Shoichet, M. S. Hydrogel for Simultaneous Tunable Growth Factor Delivery and Enhanced Viability of Encapsulated Cells in Vitro. Biomacromolecules 2016, 17, 476–484.

(46) McKinnon, D. D.; Domaille, D. W.; Cha, J. N.; Anseth, K. S. Bis-Aliphatic Hydrazone-Linked Hydrogels Form Most Rapidly at Physiological pH: Identifying the Origin of Hydrogel Properties with Small Molecule Kinetic Studies. Chem. Mater. 2014, 26, 2382–2387.

(47) Adroher-Benítez, I.; Martin-Molina, A.; Ahualli, S.; QuesadaPerez, M.; Odriozola, G.; Moncho Jorda, A. Competition between Excluded-Volume and Electrostatic Interactions in Nanogels Swelling: Effect of the Counterion Valence and Nanogel Charge. Phys. Chem. Chem. Phys. 2017, 19, 6838–6848.

(48) Su, J.; Hu, B.-H.; Lowe, W. L.; Kaufman, D. B.; Messersmith, P. B. Anti-Inflammatory Peptide-Functionalized Hydrogels for InsulinSecreting Cell Encapsulation. Biomaterials 2010, 31, 308–314.

(49) Nicodemus, G. D.; Bryant, S. J. Cell Encapsulation in Biodegradable Hydrogels for Tissue Engineering Applications. Tissue Eng., Part B 2008, 14, 149–165.

(50) O'Cearbhaill, E.; Ng, K.; Karp, J. Emerging medical devices for inimally invasive cell therapy. Mayo Clin. Proc. 2014, 89, 259–273.

(51) Samal, S. K.; Dash, M.; Van Vlierberghe, S.; Kaplan, D. L.; Chiellini, E.; van Blitterswijk,

C.; Moroni, L.; Dubruel, P. Cationic Polymers and Their Therapeutic Potential. Chem. Soc. Rev. 2012, 41, 7147–7194.

(52) Lavik, E. B.; Klassen, H.; Warfvinge, K.; Langer, R.; Young, M. J. Fabrication of Degradable Polymer Scaffolds to Direct the Integration and Differentiation of Retinal Progenitors. Biomaterials 2005, 26, 3187–3196.

(53) Brodbeck, W. G.; Nakayama, Y.; Matsuda, T.; Colton, E.; Ziats, N. P.; Anderson, J. M. Biomaterial surface chemistry dictates adherent monocyte/macrophage cytokine expression in vitro. Cytokine+ 2002, 18, 311–319.

(54) Tang, L.; Thevenot, P.; Hu, W. Surface chemistry influences implant biocompatibility. Curr. Top. Med. Chem. 2008, 8, 270–280.

(55) Mathur, A. M.; Drescher, B.; Scranton, A. B.; Klier, J. Polymeric Emulsifiers Based on Reversible Formation of Hydrophobic Units. Nature 1998, 392, 367–370.

(56) Keselowsky, B. G.; Collard, D. M.; García, A. J. Integrin binding specificity regulates biomaterial surface chemistry effects on cell differentiation. Proc. Natl. Acad. Sci. U. S. A. 2005, 102, 5953–5957.

(57) Schwartz, M. A. Integrin signaling revisited. Trends Cell Biol. 2001, 11, 466–470.